Journal of Electrochemistry

Volume 25
Issue 4 *Special Issue: Electrochemical Reduction of Carbon Dioxide*

2019-08-28

Electrocatalytic Reduction of Carbon Dioxide to Carbon Monoxide using Cobalt Nitride

Chen MA

Peng-fei HOU

Peng KANG
School of Chemical Engineering and Technology, Tianjin University, Tianjin 300072, China),
kang.peng@tju.edu.cn

Recommended Citation
Chen MA, Peng-fei HOU, Peng KANG. Electrocatalytic Reduction of Carbon Dioxide to Carbon Monoxide using Cobalt Nitride[J]. *Journal of Electrochemistry*, 2019 , 25(4): 180941.
DOI: 10.13208/j.electrochem.180941
Available at: https://jelectrochem.xmu.edu.cn/journal/vol25/iss4/6

DOI: 10.13208/j.electrochem.180941
Cite this: *J. Electrochem.* **2019**, *25*(4): 467-476

Artical ID:1006-3471(2019)04-0467-10
Http://electrochem.xmu.edu.cn

Electrocatalytic Reduction of Carbon Dioxide to Carbon Monoxide using Cobalt Nitride

MA Chen[1,2], HOU Peng-fei[1,2], KANG Peng[1,2,3*]

(1. *Key Laboratory of Photochemical Conversion and Optoelectronic Materials, Technical Institute of Physics and Chemistry, Beijing* 100190, *China*; 2. *University of Chinese Academy of Sciences, Chinese Academy of Sciences, Beijing* 100190, *China*; 3. *School of Chemical Engineering and Technology, Tianjin University, Tianjin* 300072, *China*)

Abstract: Electrocatalytic reduction of carbon dioxide (CO_2) is a promising method to alleviate global warming issues, although it still faces many challenges. Herein, we report cobalt nitride for electrocatalytic reduction of CO_2 to carbon monoxide (CO) in an aqueous electrolyte. A comparison of catalysts with different preparation temperatures and atmospheres suggests that nitrogen doping is critical to improve catalytic activity. For the most active catalyst of 700-$Co_{5.47}N$/C, the CO current density reached 9.78 $mA\cdot cm^{-2}$ at potential of -0.7 V vs. RHE. In addition, the CO/H_2 ratio could be adjusted from 1:3 to 3:2 by changing applied potential. Tafel slope of 91 $mV\cdot dec^{-1}$ indicates that forming a surface adsorbed $CO_2^{\cdot -}$ intermediate became the rate-determining step and nitriding strategy increased CO_2 selectivity by providing more base sites.

Key words: cobalt nitride; carbon dioxide electroreduction; carbon monoxide; syngas

CLC Number: O646 **Document Code:** A

The greenhouse effect becomes more prominent with increasing concentrations of CO_2 in atmosphere[1]. Electrocatalytic reduction of CO_2 (CO_2RR) is a promising method that converts CO_2 to useful fuels or chemicals such as CO, CH_4, HCOOH and other molecules[2]. Unfortunately, high overpotential, low product selectivity and short catalyst durability have hindered the application of CO_2RR[3-7]. Many metal electrocatalysts such as Au, Ag and Pd-based electrocatalysts have been used for CO_2RR[3, 8-15]. Although those catalysts have shown high selectivity and durability with low overpotential, high cost urges to develop new catalysts of abundant and inexpensive materials[16-19]. First-row transitional metals have open d orbitals, and can easily accept electrons for electrochemical reactions[20]. Moreover, they are not constrained by price and content. Therefore, first-row transitional metals have been explored for water oxidation and oxygen reduction reactions, etc.

Transition metal nitrides exhibit good catalysis performance in many important reactions[21-25]. The alloyed Co-M nitride electrocatalyst was reported with decent performance for oxygen reduction and water oxidation reactions. Tantalum cobalt nitride photocatalysts showed 12 times higher photocurrent than Ta_3N_5 for water oxidation under visible light[26], as cobalt nitride efficiently facilitates electron transfer and suppresses recombination of photogenerated electron-hole pairs. The Co-Mo nitride electrocatalyst shows great potential for fuel cells[22]. Metallic Co_4N nanowire arrays on carbon cloth can be an active oxygen evolution elelctrocatalyst[27].

Recent reports indicate that N-doping is beneficial to CO_2 reduction reaction and plays an important role in this reaction[28-31]. N-doping increases surface base sites, which makes CO_2 adsorption on surface more easily. In addition, more active sites could be formed for CO_2 reduction reaction[32].

Received: 2018-10-08, Revised: 2018-12-16 *Corresponding author, Tel: (86)18511115777, E-mail: kang.peng@tju.edu.cn

From the above reports, cobalt nitrides are promising electrocatalysts for CO_2 reduction. However, few reports of cobalt nitrides are known for carbon dioxide reduction. Recently, CoN wrapped with N-doped carbon (CoN/N-C) nanocatalysts presented excellent photoelectrocatalytic activity toward CO_2 reduction with high CO selectivity[33]. However, the activity of CO_2 electroreduction has not been fully investigated.

1 Experimental

1.1 Chemicals and Apparatus

$NaHCO_3$ (99.5%) and ethanol (99.7%) were purchased from Beijing Chemical Works; $Co(NO_3)_2 \cdot 6H_2O$ (≥98.0%) was purchased from Guanghua Chemical Co., Ltd; Ar (99.999%), and CO_2 (99.999%) were purchased from Beijing HuanYu Gases Company; NH_3 (99.999%) was purchased from Beijing Chengxinshunxing Gases Company; Nafion® 212 membrane was purchased from DuPont. All chemicals were used without further purification. Electrolyte solutions were prepared with DI water.

The morphology of catalysts was characterized by JEOL JEM-2100 transmission electron microscope (TEM). ESCALAB 250 XI X-ray photoelectron spectroscope (XPS) of Thermo Scientific was used to analyze the surface electronic structures, using a monochromatic Al K_α radiation (1486.6 eV). The binding energies were calibrated with reference to the C 1s peak at 284.6 eV. X-ray diffraction (XRD) data were collected on a Bruker DAVINCI D8 ADVANCE diffractometer using a Cu K_α source (λ = 1.54184 nm). X-ray diffraction spectra were obtained for 2θ values differing from 10 to 90 degrees with a step length of 0.1 degree.

1.2 Material Preparation

The catalysts were prepared by impregnation and nitridation method. 1 g $Co(NO_3)_2 \cdot 6H_2O$ and 0.3 g carbon black were mixed with 50 mL ethanol in a beaker equipped with a stir bar, followed by agitation in air for 24 h at room temperature. The catalyst precursor was obtained after evaporating the resulting mixture in the oil bath at 100 ℃ and dried in vacuum overnight. The catalyst precursor was put into a tubular furnace. The $Co_{5.47}N$/C catalysts were prepared by calcination of the precursor under an NH_3 atmosphere (flow rate 100 mL·min^{-1}) at different temputures of 500, 600, 700 and 800 °C for 3 h with a heating rate of 5 °C·min^{-1} and a cooling rate of 3.3 °C·min^{-1}. The four as-prepared $Co_{5.47}N$/C materials were denoted as 500-$Co_{5.47}N$/C, 600-$Co_{5.47}N$/C, 700-$Co_{5.47}N$/C and 800-$Co_{5.47}N$/C. The CoO/C catalyst was prepared by the same procedure as 700-$Co_{5.47}N$/C, except under Ar atmosphere.

1.3 Electrochemical Measurement

Electrochemical measurements were carried out in a conventional three-electrode system using 0.5 mol·L^{-1} $NaHCO_3$ aqueous electrolyte at room temperature. The Pt wire and saturated calomel reference electrode (SCE) were used as the counter electrode and reference electrode, respectively. The measured potentials after iR compensation were rescaled to RHE (reversible hydrogen standard potential) by E(vs. RHE) = E(vs. SCE) + 0.245 V + 0.0591 V × pH. All potentials in this manuscript are relative to the RHE unless otherwise stated. The working electrode was prepared as following: 10 mg catalysts and 100 μL of 5wt% Nafion solution were dispersed in 1 mL ethanol with sonication for 1 h to form a homogeneous ink. 5 μL of the ink was load onto a 3 mm diameter glassy carbon electrode and dried at room temperature before electrochemical tests. The gaseous products were analyzed by SRI MG-I GC with a helium ionization detector (HID). Liquid products were analyzed by proton NMR (Bruker AVNANCE-400) using dimethylformamide as an internal standard.

2 Results and Discussion

Cobalt nitride catalysts were prepared by temperature programmed reaction (TPR) at temperatures from 500 °C to 800 °C under an ammonia atmosphere. Fig. 1A shows the XRD patterns of cobalt nitrides prepared at different temperatures and their diffraction peaks are similar. The XRD pattern matched with JCPDS No. 41-0943, suggesting that ammonolysis is effective in forming $Co_{5.47}N$ particles[34-35]. Three peaks appeared at 43.7°, 50.9° and 75.0° could be assigned to the (111), (200) and (220) planes of $Co_{5.47}N$,

respectively, indicating that cobalt nitrides were successfully synthesized. The main diffraction peak was assigned to the (111) plane of $Co_{5.47}N$. The diffraction peaks of 700-$Co_{5.47}N$/C were sharper and stronger than those of $Co_{5.47}N$/C prepared at other nitridation temperatures, suggesting increased crystallinity. No other characteristic peaks were detected in the XRD patterns, suggesting that the purity of the samples is very high. XRD data in Fig. 1A indicates that CoO formed after the precursor was annealed under Ar at 700 ℃ for 3 h, which was used for comparison.

X-ray photoelectron spectrum was collected to analyze the surface chemical composition. The peaks of Co 2p, N 1s, O 1s and C 1s appear at the XPS spectrum (Fig. 1B). As shown in Fig. 1C, the main peaks of Co at 781.42 eV and 796.90 eV corresponded to Co $2p_{3/2}$ and Co $2p_{1/2}$, respectively. Simultaneously, the peaks at 786.31 eV and 803.74 eV were satellite peaks. These indicated that the Co atoms were Co^{2+} species[36-37]. Moreover, these two Co 2p peaks were consistent with the peaks of Co at $Co_{5.47}N$[22, 26]. The N 1s spectrum showed four types of N atoms in Fig. 1D. According to previous works, the peak at 397.84 eV resulted from N-Co bond[22]. In addition, the peaks at 398.58, 400.29 and 401.23 eV corresponded to pyridinic N, pyrrolic N and graphitic N,

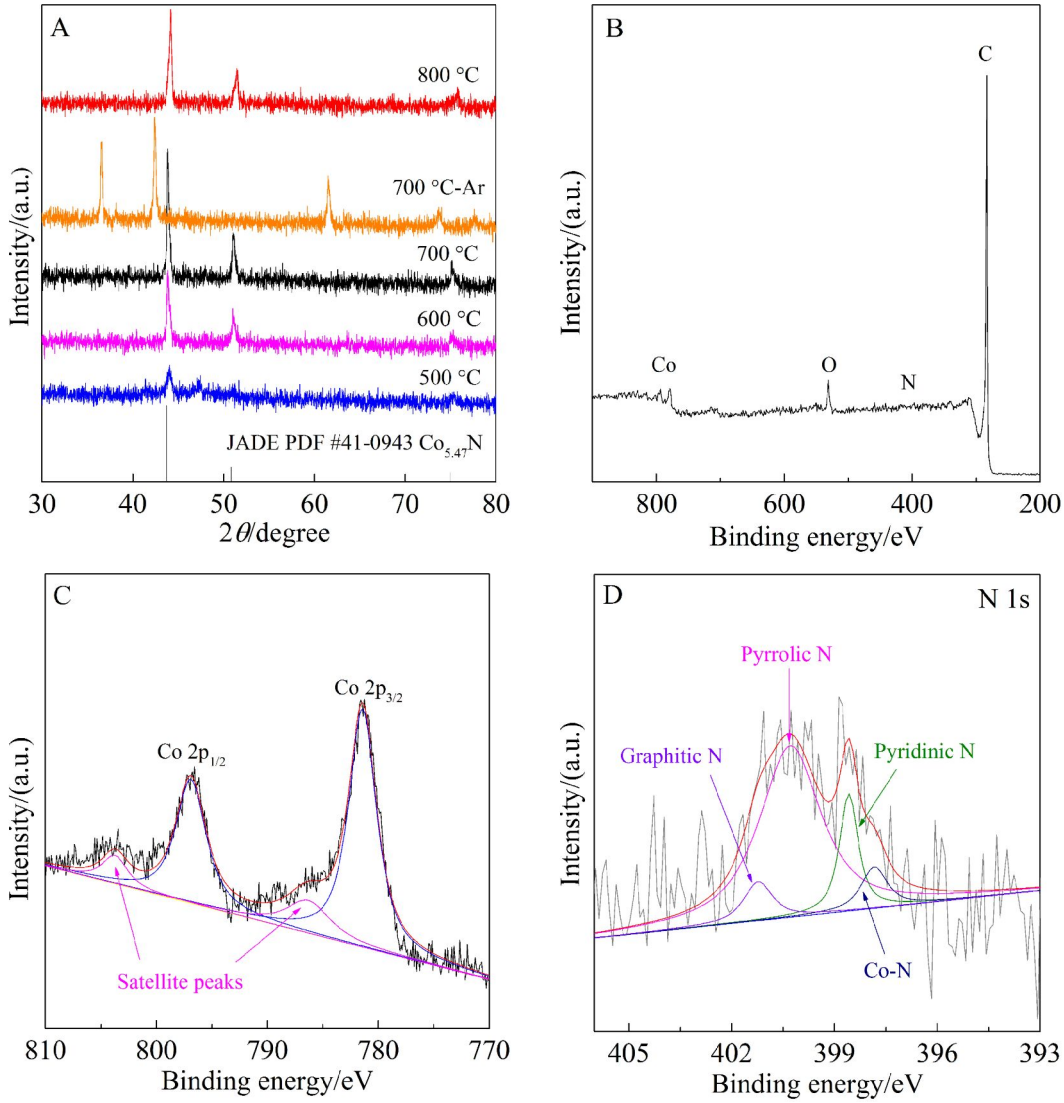

Fig. 1 (A) XRD patterns of the $Co_{5.47}N$/C catalysts and CoO/C, and XPS spectra of 700-$Co_{5.47}N$/C for survey (B), Co 2p (C) and N 1s (D).

respectively[38]. Together, these results indicated that $Co_{5.47}N$ particles were synthesized successfully.

The transmission electron microscopy (TEM) was used to examine microstructure of materials. As shown in Fig. 2, the cobalt nitride nanoparticles were uniformly distributed on the XC-72R carbon black (denoted as C) with average diameter of ca. 20 nm. The HRTEM image in Fig. 2D shows a lattice spacing of 0.207 nm, which corresponds to the (111) plane of $Co_{5.47}N$. The TEM image in Fig. 2E shows CoO/C of ca. 120 nm in average.

The activity of $Co_{5.47}N$/C for CO_2 reduction was evaluated using cyclic voltammetry (CV) and controlled potential electrolysis. As shown in Fig. 3C, the onset potential was at -0.3 V and subsequently current density increased rapidly. Moreover, the current density at CO_2 saturated aqueous solutions was ca. two times higher than that under Ar at potentials ranging from -0.4 to -0.8 V. The increase stemmed from CO_2 reduction reaction on 700-$Co_{5.47}N$/C. In addition, there was no obvious current for CO_2 reduction when using nitrided carbon black as a control sample (Fig. 3E). It suggests that nitrided carbon black did not contribute significantly to the catalytic currents for CO_2 reduction reaction. Also, there was no significant catalytic current when using CoO/C for CO_2 reduction at the same condition (Fig. 3F).

Controlled potential electrolysis was performed to investigate the product distribution in CO_2-saturated $NaHCO_3$ aqueous electrolyte. Gas chromatograph and NMR were used to analyze gas-phase and liquid products, respectively. CO and H_2 were the primary gaseous products and no liquid products were detected. As shown in Fig. 3, volcano curves of CO faradaic efficiency were obtained at potentials ranging from -0.4 to -0.8 V. 700-$Co_{5.47}N$/C showed the highest faradaic efficiency for CO of 59.1% at -0.6 V, corresponding to 0.5 V overpotential.

For 700-$Co_{5.47}N$/C, the CO faradaic efficiency increased quickly with further applied potential. The maximum CO faradaic efficiencies were 40.4% , 47.8% and 59.9% for 500-, 600- and 700-$Co_{5.47}N$/C at -0.6 V, respectively. However, for 800-$Co_{5.47}N$/C, the maximum faradaic efficiency for CO was only 39.4%

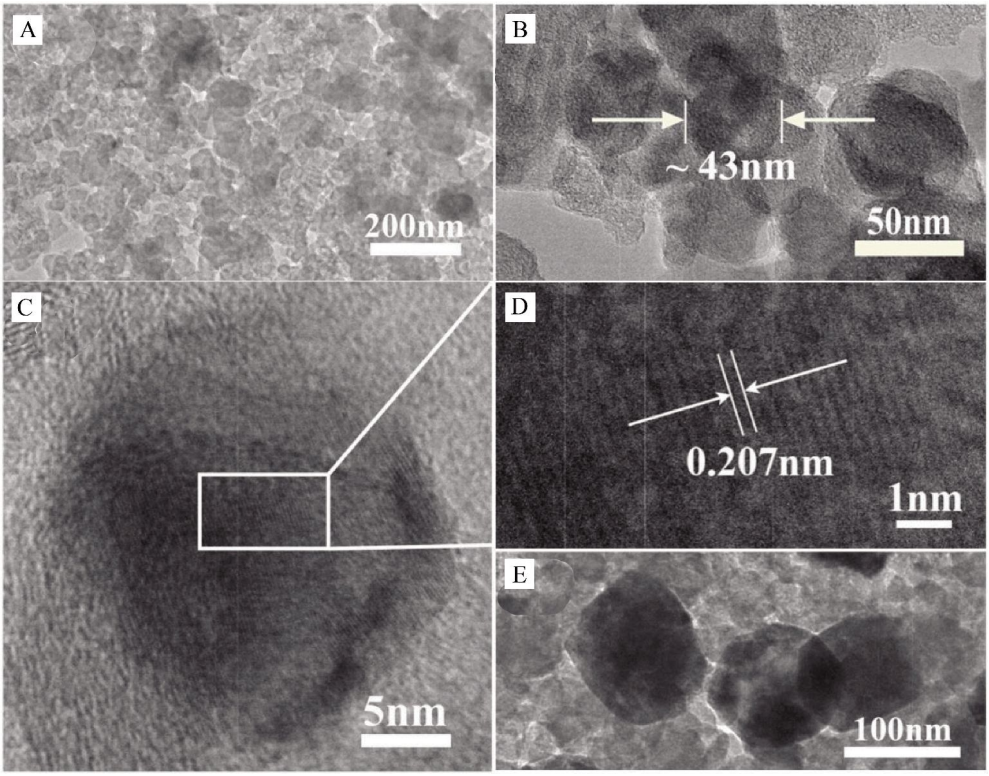

Fig. 2 TEM images. (A), (B), (C) and (D) 700-$Co_{5.47}N$/C, and (E) CoO/C.

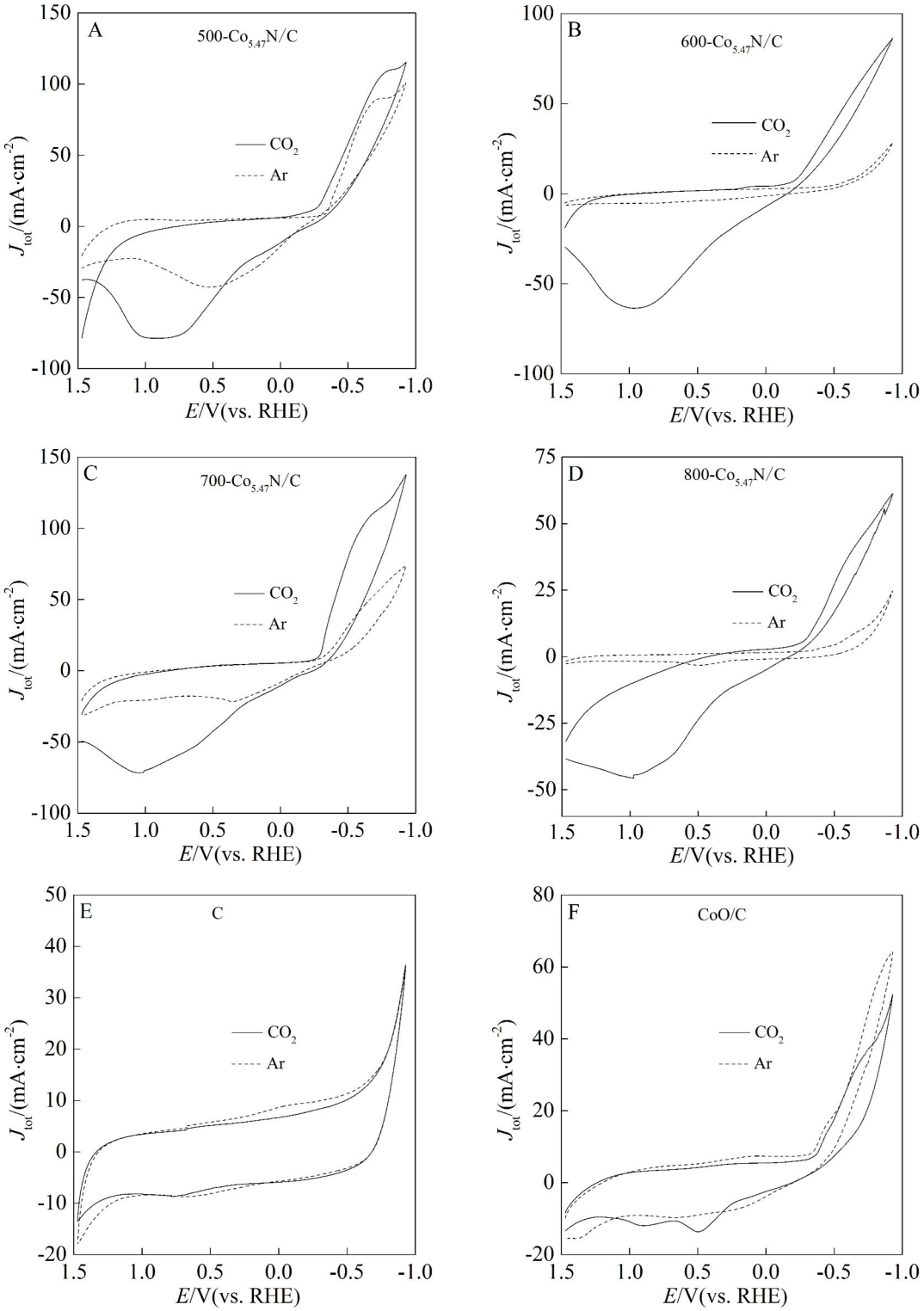

Fig. 3 CV scans of (A) 500-$Co_{5.47}$N/C, (B) 600-$Co_{5.47}$N/C, (C) 700-$Co_{5.47}$N/C, (D) 800-$Co_{5.47}$N/C, (E) carbon black and (F) CoO/C under CO_2 (solid) and Ar (dashed) in 0.5 mol·L^{-1} $NaHCO_3$ saturated aqueous solution, scan rate: 50 mV·s^{-1}.

at -0.7 V. A further increase in applied potentials resulted in a sharp decrease in the CO faradaic efficiencies. This may be due to mass transport limitations of CO_2 at high overpotential. By contrast, the faradaic efficiencies of CoO/C prepared at different temperatures for producing CO were nearly 0%. These data

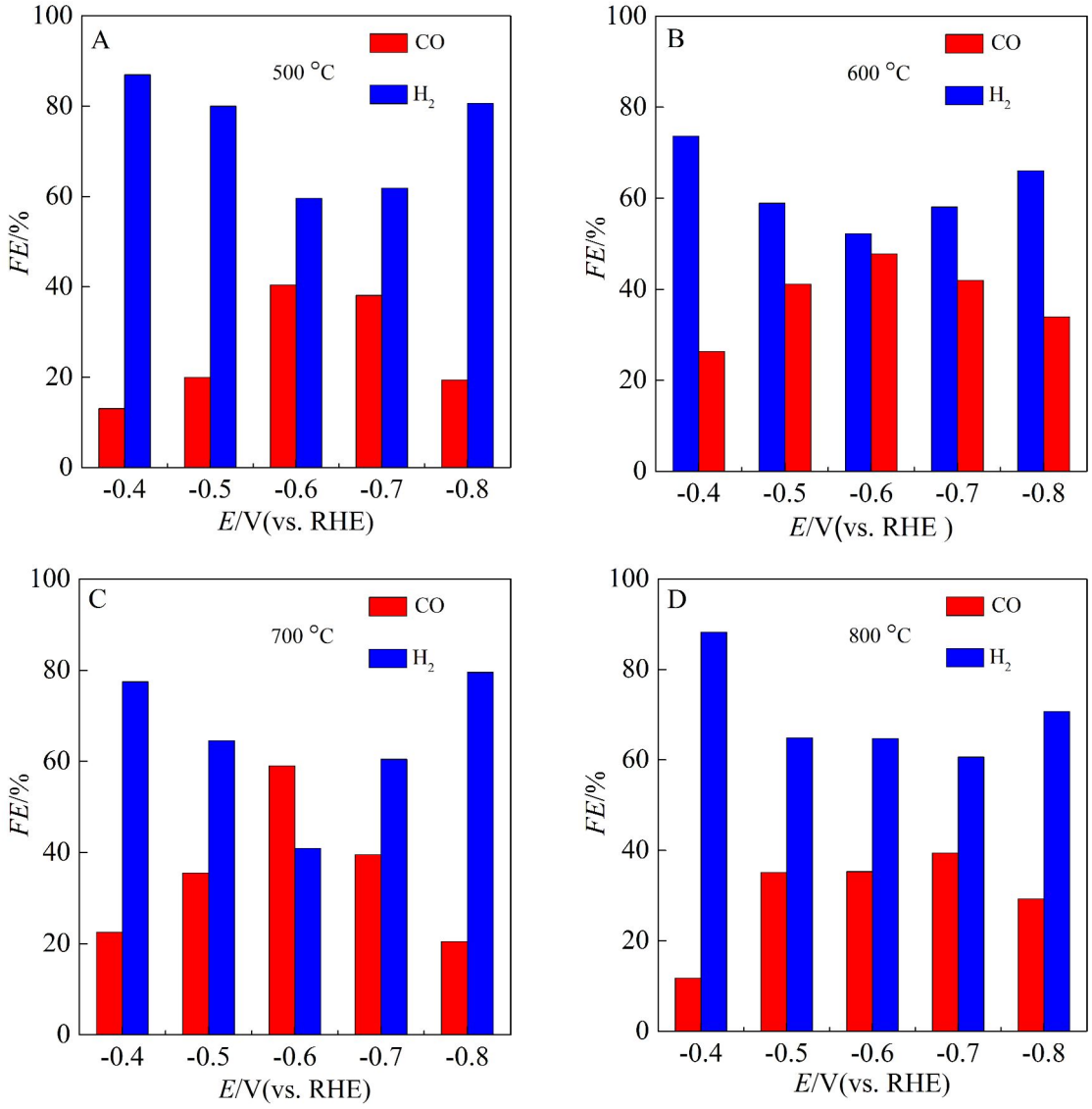

Fig. 4 Faradaic efficiency vs. applied potential for $Co_{5.47}N/C$ prepared at different temperatures. (A) 500 ℃, (B) 600 ℃, (C) 700 ℃, (D) 800 ℃. The CO_2 electrochemical reduction (CO_2RR) occurred in CO_2-saturated 0.5 mol·L^{-1} $NaHCO_3$.

imply that CoO/C is not an effective catalyst for CO_2RR.

Fig. 5A illustrates the dependence of CO current density on the applied electrolysis potential for $Co_{5.47}N/C$ prepared at different temperatures. Apparently, 700-$Co_{5.47}N/C$ achieved the maximum CO current density of 9.8 mA·cm^{-2} at -0.7 V. The CO current densities increased at the potentials ranging from -0.4 to -0.7 V, but then decreased at more negative potentials.

Changing the nitride temperature allowed tuning of the CO/H_2 ratio in the product from 0.55 to 1.44 at -0.6 V as evident in Fig. 5B. Moreover, the highest CO/H_2 ratio of 1.44 was obtained with 700-$Co_{5.47}N/C$ which showed an increase in the CO/H_2 ratio from 0.3 to 1.44 by varying the potentials from -0.4 to -0.6 V, corresponding to the increased CO faradaic efficiency from 22.5% to 59.1%. Fig. 5C shows high catalyst stability for 700-$Co_{5.47}N/C$ at -0.6 V. During the 10-h electrolysis, the CO faradaic efficiency maintained at 55%, which implies that the catalyst did not degrade to metallic Co.

The preparation temperature influences the crystallinity and morphology of catalyst, causing the dif-

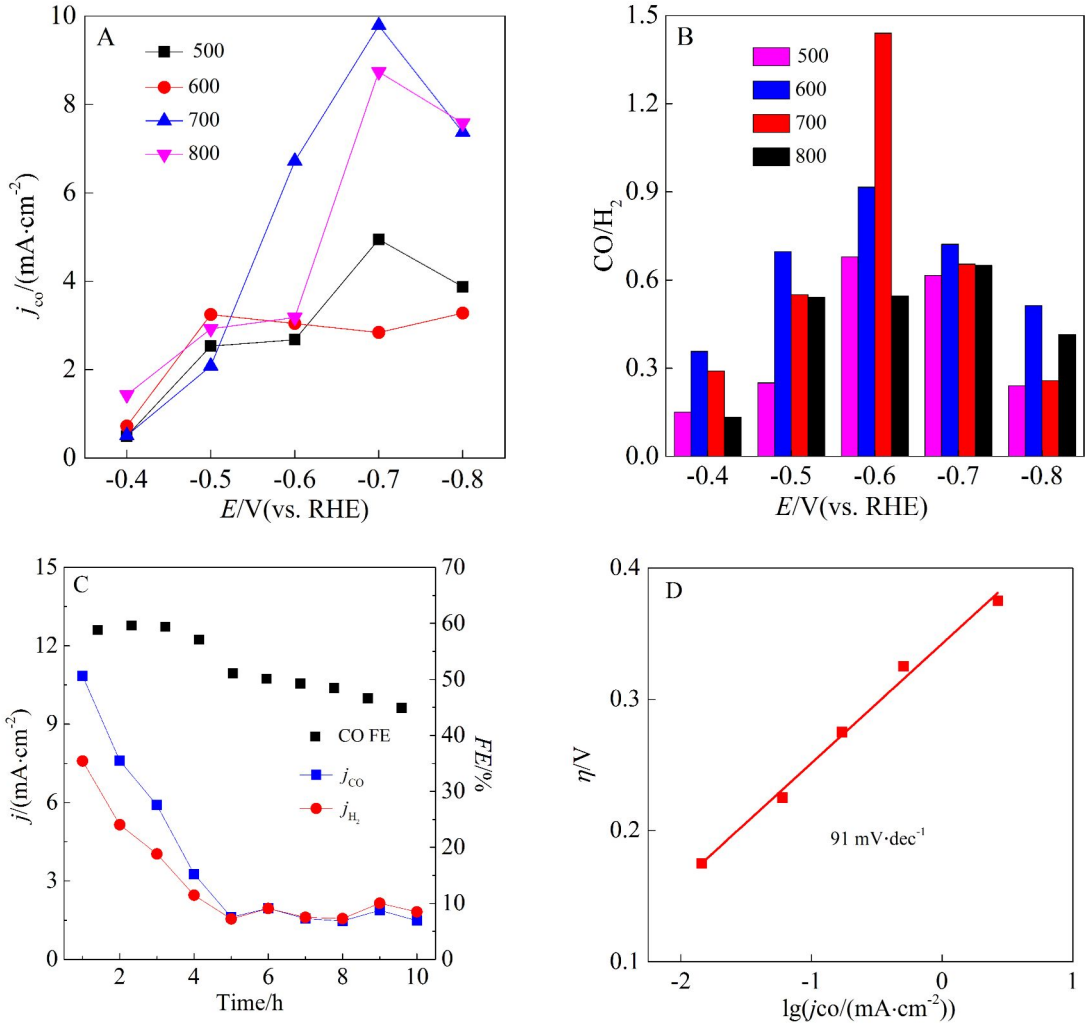

Fig. 5 (A) CO current density and (B) CO/H_2 vs. applied potential as a function of potential. (C) CO FE, CO and H_2 current densities vs. time for 700-$Co_{5.47}N$ at -0.6 V vs. RHE in CO_2-saturated 0.5 mol·L^{-1} $NaHCO_3$. (D) Tafel plot using CO partial current density for 700-$Co_{5.47}N$/C.

ference in the selectivity for CO production. As the preparation temperature increased from 500 to 700 ℃, the crystallinity of catalyst enhanced. This may be the reason that 700-$Co_{5.47}N$/C shows higher selectivity and current density for CO production than 500-$Co_{5.47}N$/C and 600-$Co_{5.47}N$/C. In addition, higher preparation temperature accelerates the agglomeration of catalyst, causing the decrease of CO selectivity.

In order to understand how CO_2 reduction works on 700-$Co_{5.47}N$/C surface, Tafel plot for CO production was obtained and is presented in Fig. 5D. Again, 700-$Co_{5.47}N$/C exhibited a slope of 91 mV·dec^{-1}, close to 118 mV·dec^{-1}. Mechanism for CO_2 reduction to CO can be inferred. The two-electron reduction of CO_2 to CO on 700-$Co_{5.47}N$/C surface includes two key steps. In the first step, surface adsorbed CO_2 obtained one electron to form a $CO_2^{\cdot -}$ intermediate. In subsequent steps, the $CO_2^{\cdot -}$ intermediate takes two protons and another electron, and forms a CO and a H_2O molecules[3]. Previous studies suggest that forming a surface adsorbed $CO_2^{\cdot -}$ intermediate needs more negative potential than the steps afterwards, and therefore, this step is the rate-determining step (RDS) of the CO_2 reduction reaction to CO.

The doping of N atoms in $Co_{5.47}N$ as a base site can facilitate the adsorption of CO_2 molecule on the surface of catalysts. This is beneficial to the activation of CO_2, which can favor the reduction of CO_2. It

is possible that cobalt nitride contains more base sites than cobalt oxide, and thus, stabilizes $CO_2^{\cdot -}$ more effectively. In addition, the first-row transitional metal Co has open d orbitals, and can transfer electrons for CO_2 reduction reaction[20].

3 Conclusions

In summary, the $Co_{5.47}N$/C particles synthesized by ammonolysis exhibited high faradaic efficiency for the reduction of CO_2 to CO and the CO current density reached 9.78 mA·cm^{-2} with low overpotential. Moreover, the CO/H_2 ratio could be adjusted from 1:3 to 3:2 by tuning the potentials of electrolysis. Furthermore, this catalyst showed good stability and could work for ca. 10 hours with high CO and H_2 faradaic efficiencies. This approach could be applicable for a variety of metal catalysts.

Acknowledgments

This work was financially supported by the National Key Projects for Fundamental Research and Development of China (2016YFB0600901), and National Nature Science Foundation of China (21701180).

References:

[1] Peltier W R, Tushingham A M. Global sea level rise and the greenhouse effect: might they be connected?[J]. Science, 1989, 244(4906): 806-810.

[2] Qiao J L, Liu Y Y, Hong F, et al. A review of catalysts for the electroreduction of carbon dioxide to produce low-carbon fuels[J]. Chemical Society Reviews, 2014, 43(2): 631-675.

[3] Lu Q, Rosen J, Zhou Y, et al. A selective and efficient electrocatalyst for carbon dioxide reduction[J]. Nature Communications, 2014, 5: 3242.

[4] Kim C, Jeon H S, Eom T, et al. Achieving selective and efficient electrocatalytic activity for CO_2 reduction using immobilized silver nanoparticles[J]. Journal of the American Chemical Society, 2015, 137(43): 13844-13850.

[5] Chen Y H, Li C W, Kanan M W. Aqueous CO_2 reduction at very low overpotential on oxide-derived Au nanoparticles[J]. Journal of the American Chemical Society, 2012, 134(49): 19969-19972.

[6] Zhu W L, Zhang Y J, Zhang H Y, et al. Active and selective conversion of CO_2 to CO on ultrathin Au nanowires [J]. Journal of the American Chemical Society, 2014, 136 (46): 16132-16135.

[7] Zhu D D, Liu J L, Qiao S Z. Recent advances in inorganic heterogeneous electrocatalysts for reduction of carbon dioxide[J]. Advanced Materials, 2016, 28(18): 3423-3452.

[8] Mistry H, Reske R, Zeng Z H, et al. Exceptional size-dependent activity enhancement in the electroreduction of CO_2 over Au nanoparticles[J]. Journal of the American Chemical Society, 2014, 136(47): 16473-16476.

[9] Zhu W L, Michalsky R, Metin O, et al. Monodisperse Au nanoparticles for selective electrocatalytic reduction of CO_2 to CO[J]. Journal of the American Chemical Society, 2013, 135(45): 16833-16836.

[10] Sun K, Cheng T, Wu L N, et al. Ultrahigh mass activity for carbon dioxide reduction enabled by gold-iron core-shell nanoparticles[J]. Journal of the American Chemical Society, 2017, 139(44): 15608-15611.

[11] Ma M, Trzesniewski B J, Xie J, et al. Selective and efficient reduction of carbon dioxide to carbon monoxide on oxide-derived nanostructured silver electrocatalysts[J]. Angewandte Chemie International Edition, 2016, 55(33): 9748-9752.

[12] Lim H K, Shin H, Goddard W A, et al. Embedding covalency into metal catalysts for efficient electrochemical conversion of CO_2[J]. Journal of the American Chemical Society, 2014, 136(32): 11355-11361.

[13] Feng X F, Jiang K L, Fan S S, et al. Grain-boundary-dependent CO_2 electroreduction activity[J]. Journal of the American Chemical Society, 2015, 137(14): 4606-4609.

[14] Gao D F, Zhou H, Wang J, et al. Size-dependent electrocatalytic reduction of CO_2 over Pd nanoparticles[J]. Journal of the American Chemical Society, 2015, 137 (13): 4288-4291.

[15] Jiang B(蒋孛), Zhang L N(张莉娜), Qin X F(秦先贤), et al. Electrodesosition of RuO_2 layers on TiO_2 nanotube array toward CO_2 Electroreduction[J]. Journal of Electrochemistry(电化学), 2017, 23(2): 238-244.

[16] Rahaman M, Dutta A, Zanetti A, et al. Electrochemical reduction of CO_2 into multicarbon alcohols on activated Cu mesh catalysts: An identical location (IL) study[J]. ACS Catalysis, 2017, 7(11): 7946-7956.

[17] Nie X W, Esopi M R, Janik M J, et al. Selectivity of CO_2 reduction on copper electrodes: the role of the kinetics of elementary steps[J]. Angewandte Chemie International Edition, 2013, 52(9): 2459-2462.

[18] Ma M, Djanashvili K, Smith W A. Controllable hydrocarbon formation from the electrochemical reduction of CO_2 over Cu nanowire arrays[J]. Angewandte Chemie International Edition, 2016, 55(23): 6679-6683.

[19] Zhao C C(赵晨辰), Guo J W(郭建伟), Wang L(王莉), et al. Electrochemical reduction of CO_2 on Sn/Cu electrode [J]. Journal of Electrochemistry(电化学), 2012, 18(2): 169-173.

[20] Meganathan M D, Mao S, Huang T Z, et al. Reduced graphene oxide intercalated Co_2C or Co_4N nanoparticles as an efficient and durable fuel cell catalyst for oxygen reduction[J]. Journal of Materials Chemistry A, 2017, 5 (6): 2972-2980.

[21] Costentin C, Robert M, Saveant J M. Catalysis of the electrochemical reduction of carbon dioxide[J]. Chemical Society Reviews, 2013, 42(6): 2423-2436.

[22] Sun T, Wu Q, Che R C, et al. Alloyed Co-Mo nitride as high-performance electrocatalyst for oxygen reduction in acidic medium[J]. ACS Catalysis, 2015, 5(3): 1857-1862.

[23] Ham D J, Lee J S. Transition metal carbides and nitrides as electrode materials for low temperature fuel cells[J]. Energies, 2009, 2(4): 873-899.

[24] Jiang M X(姜孟秀), Zhang J(张晶), Li Y H(李月华), et al. Cobalt-based nitrogen-doped carbon non-noble metal catalysts for oxygen reduction reaction[J]. Journal of Electrochemistry (电化学), 2017, 23(6): 627-637.

[25] Zhang Y(张雅琳), Chen C(陈驰), Zou L L(邹亮亮), et al. Fe-N doped hollow carbon nanospheres linked by carbon nanotubes for oxygen reduction reaction[J]. Journal of Electrochemistry (电化学), 2017, 24(60): 726-732.

[26] Cong Y, Park H S, Dang H X, et al. Tantalum cobalt nitride photocatalysts for water oxidation under visible light[J]. Chemistry of Materials, 2012, 24(3): 579-586.

[27] Chen P Z, Xu K, Fang Z W, et al. Metallic Co_4N porous nanowire arrays activated by surface oxidation as electrocatalysts for the oxygen evolution reaction[J]. Angewandte Chemie International Edition, 2015, 54(49): 14710-14714.

[28] Jhong H R M, Tornow C E, Smid B, et al. A nitrogen-doped carbon catalyst for electrochemical CO_2 conversion to CO with high selectivity and current density [J]. ChemSusChem, 2017, 10(6): 1094-1099.

[29] Song Y F, Chen W, Zhao C C, et al. Metal-free nitrogen-doped mesoporous carbon for electroreduction of CO_2 to ethanol[J]. Angewandte Chemie International Edition, 2017, 129(36): 10980-10984.

[30] Sun X F, Kang X C, Zhu Q G, et al. Very highly efficient reduction of CO_2 to CH_4 using metal-free N-doped carbon electrodes[J]. Chemical Science, 2016, 7(4): 2883-2887.

[31] Zhang S, Kang P, Ubnoske S, et al. Polyethylenimine-enhanced electrocatalytic reduction of CO_2 to formate at nitrogen-doped carbon nanomaterials[J]. Journal of the American Chemical Society, 2014, 136(22): 7845-7848.

[32] Liu Y n, Zhang Y J, Cheng K, et al. Selective electrochemical reduction of carbon dioxide to ethanol on a boron and nitrogen-Co-doped nanodiamond[J]. Angewandte Chemie International Edition, 2017, 56(49): 15607-15611.

[33] Weng B C, Wei W, Yiliguma, et al. Bifunctional CoP and CoN porous nanocatalysts derived from ZIF-67 *in situ* grown on nanowire photoelectrodes for efficient photo electrochemical water splitting and CO_2 reduction[J]. Journal of Materials Chemistry A, 2016, 4(40): 15353-15360.

[34] Zhang L, Deng Y, Yu J Y, et al. Synthesis and properties of $Co_{5.47}N$ thin films by chemical solution deposition[J]. Materials Letters, 2018, 225: 145-148.

[35] Ding L, Hu S S, Quan X M, et al. Effect of VN alloy addition on the microstructure and wear resistance of Co-based alloy coatings[J]. Journal of Alloys and Compounds, 2016, 659: 8-14.

[36] Barreca D, Massignan C, Daolio S, et al. Composition and microstructure of cobalt oxide thin films obtained from a novel cobalt(II) precursor by chemical vapor deposition[J]. Chemistry of Materials, 2001, 13(2): 588-593.

[37] Li S, Zhang L, Kim J, et al. Synthesis of carbon-supported binary FeCo-N non-noble metal electrocatalysts for the oxygen reduction reaction[J]. Electrochimica Acta, 2010, 55(24): 7346-7353.

[38] Chen S, Bi J Y, Zhao Y, et al. Nitrogen-doped carbon nanocages as efficient metal-free electrocatalysts for oxygen reduction reaction[J]. Advanced Materials, 2012, 24(41): 5593-5597.

氮化钴电催化还原二氧化碳为一氧化碳

马 晨[1,2], 侯朋飞[1,2], 康 鹏[1,2,3*]

(1. 中国科学院理化技术研究所,中国科学院光化学转换与功能材料重点实验室,北京 100190;
2. 中国科学院大学,北京 100190;3. 天津大学化工学院, 天津 300072)

摘要:电催化还原二氧化碳是一种潜在的解决全球变暖的途径,但是仍有许多挑战. 本文报道了使用氮化钴在水溶液中电催化还原二氧化碳为一氧化碳. 通过对比不同煅烧温度及气氛合成的催化剂表明氮掺杂对催化活性的提高至关重要. 其中 700-$Co_{5.47}$N/C 展现了最高的催化活性,在较低的电势 -0.7 V(vs. RHE)下,一氧化碳的电流密度达到 9.78 mA·cm^{-2}. 另外, 通过改变电解电压,CO/H_2 的比例能在 1:3 到 3:2 之间调节. 91 mV·dec^{-1} 的 Tafel 斜率表明形成表面吸附的 $CO_2^{\cdot-}$中间体是 CO_2 表面还原的决速步骤,而氮化策略可以增加表面碱性位点的数量,从而稳定还原的中间体,提高反应效率和产物选择性.

关键词: 氮化钴;二氧化碳电还原;一氧化碳;合成气